Supplementary Information

Tuning material properties via disorder: from crystalline alloy to metallic glass

A. Troglia[1], V. Vollema[1], S. Cassanelli[2], E. van Heumen[2], J. van de Groep[2], A. de Visser[2] and R. Bliem[1, 2, *]

[1] *Advanced Research Center for Nanolithography, Science Park 106, 1098 XG Amsterdam, The Netherlands*

[2] *Van der Waals–Zeeman Institute, University of Amsterdam, Science Park 904, 1098 XH Amsterdam, The Netherlands*

[*] *r.bliem@arcnl.nl*

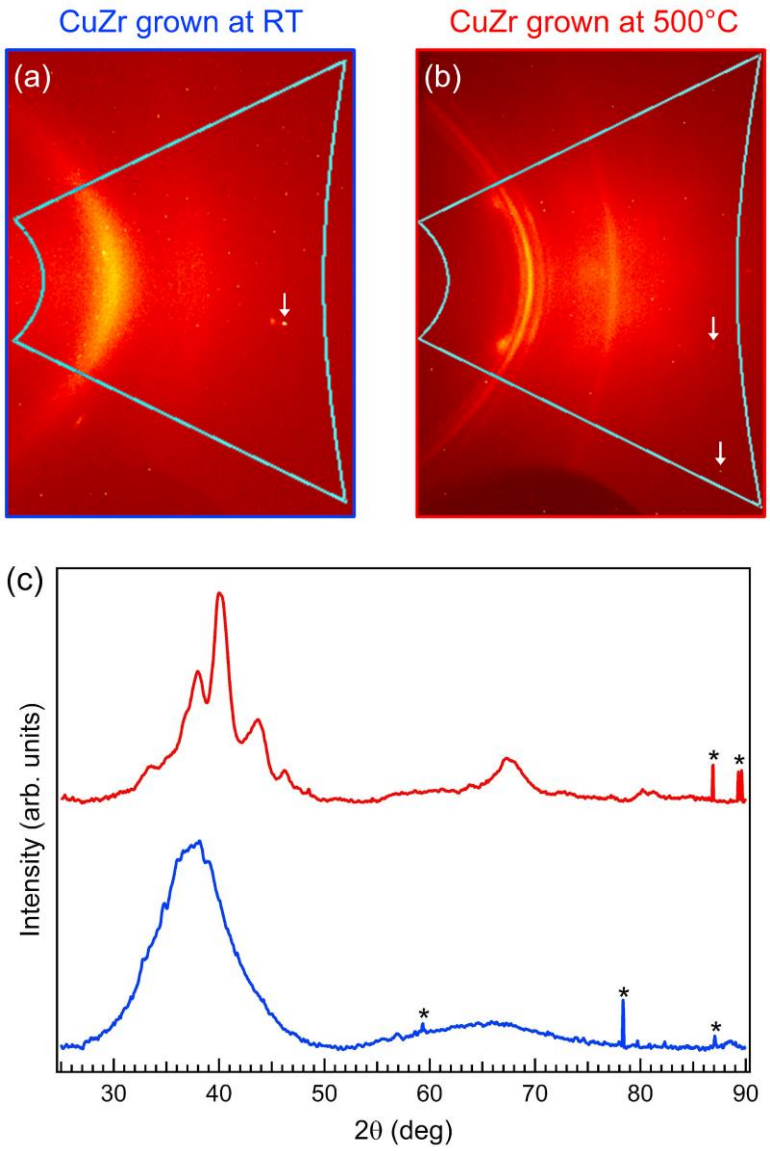

Figure S1: 2D diffraction patterns corresponding to CuZr thin films grown at RT (a) and at 500°C (b). The integration of the area marked with a light blue line allowed to extract the diffractograms reported in (c). The sharp spikes marked with an asterisk in (c) are artefacts of the measurement ascribed to saturated pixels on the 2D detector (indicated in (a) and (b) with white arrows). These artefacts have been removed in Figure 1 of the main text.

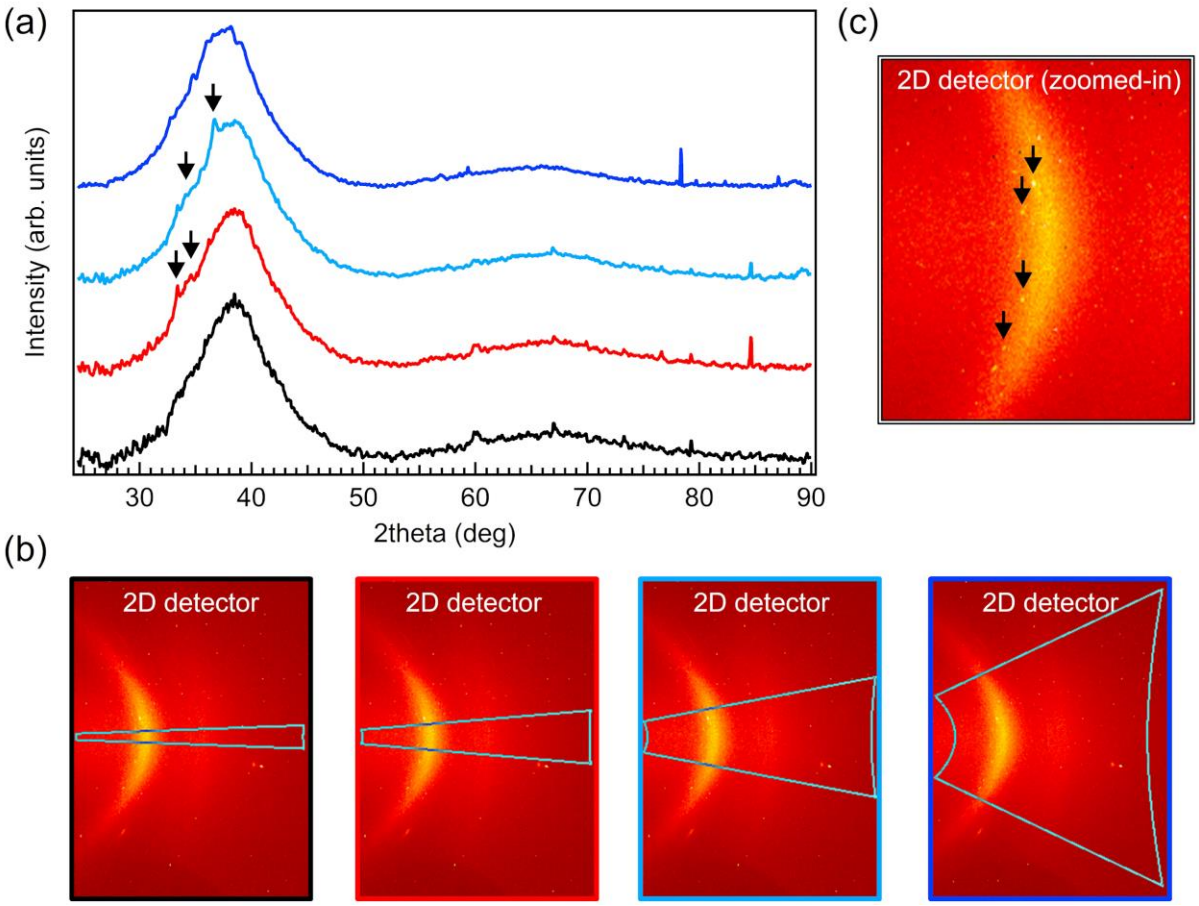

Figure S2 (a) GI-XRD diffractograms of a CuZr thin film deposited at room temperature derived from a 2D diffraction pattern by integrating over different ranges of in-plane angles, indicated in (b). The sharp features marked with black arrows in (a) are ascribed to diffraction from individual crystalline droplets from melt ejection. The corresponding diffraction spots are marked with black arrows in the zoomed-in image of the 2D detector (c).

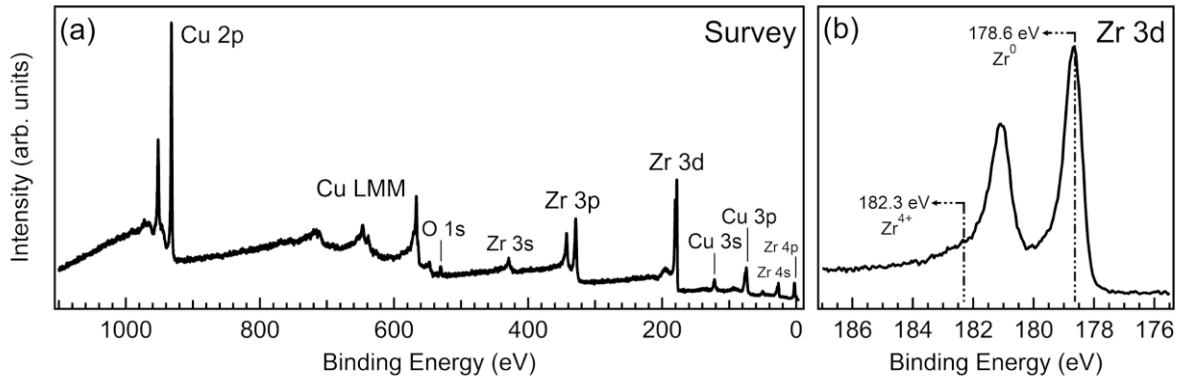

Figure S3: In-situ XPS investigation of an as-grown CuZr thin film. (a) XPS survey showing the presence of Cu, Zr and small traces of O. (b) Detailed measurement of the Zr 3d region: the main doublet is located at E_B = 178.6 eV, indicating that Zr is mostly metallic. Small traces of Zr^{4+} around E_B = 182.3 eV are visible in the tail of the Zr 3d doublet. From the measured XPS peak areas we can estimate a 5% surface contamination with oxygen. We ascribe the presence of a small amount of oxygen to the interaction of the highly reactive element Zr with water still present in the deposition and measurement vacuum chamber, despite the excellent background pressure (better than 5.0×10^{-10} mbar and 1.0×10^{-9} mbar, respectively). This is clearer by considering the as-grown XPS spectrum of the Zr 3d region shown in (b): the main Zr $3d_{5/2}$ peak is located at 178.6 eV of binding energy, in good agreement with the expected value for metallic Zr [1]*. On the other hand, the presence of a*

small contribution from ZrO_2 species around 182.3 eV [1] *is visible as a weak shoulder in the tail of the metallic Zr $3d_{3/2}$ peak. Also, the presence of small traces of sub-oxide species in the range between 179.0 eV and 182.0 eV* [1] *cannot be excluded. Nevertheless, the total oxygen content is very low, confirming the high purity of the as-grown CuZr thin films.*

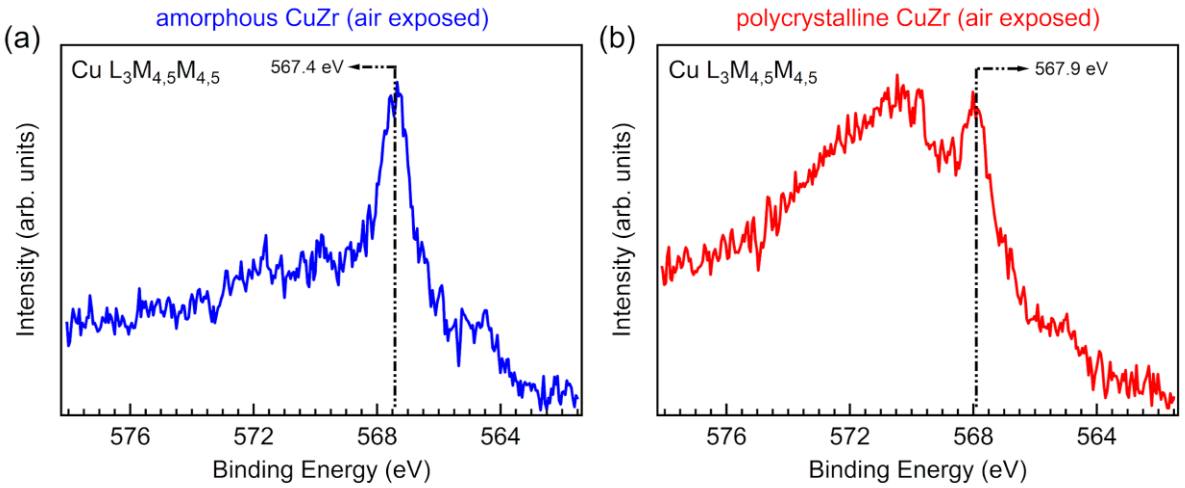

Figure S4: XPS measurements of the Cu $L_3M_{4,5}M_{4,5}$ Auger region for amorphous (a) and polycrystalline (b) CuZr thin films after air exposure. The main peak position is marked with a dashed line. The calculated Auger parameter (α'=1851.3 eV) for polycrystalline CuZr is in very good agreement with the calculated value for metallic Cu [2] *in amorphous CuZr. However, the higher spectral intensity around E_B=570 eV suggests the presence of peaks ascribed to CuO (expected at E_B~569.0 eV* [2]*) and $Cu(OH)_2$ (expected at E_B~570.4 eV* [2]*) in the polycrystalline CuZr film.*

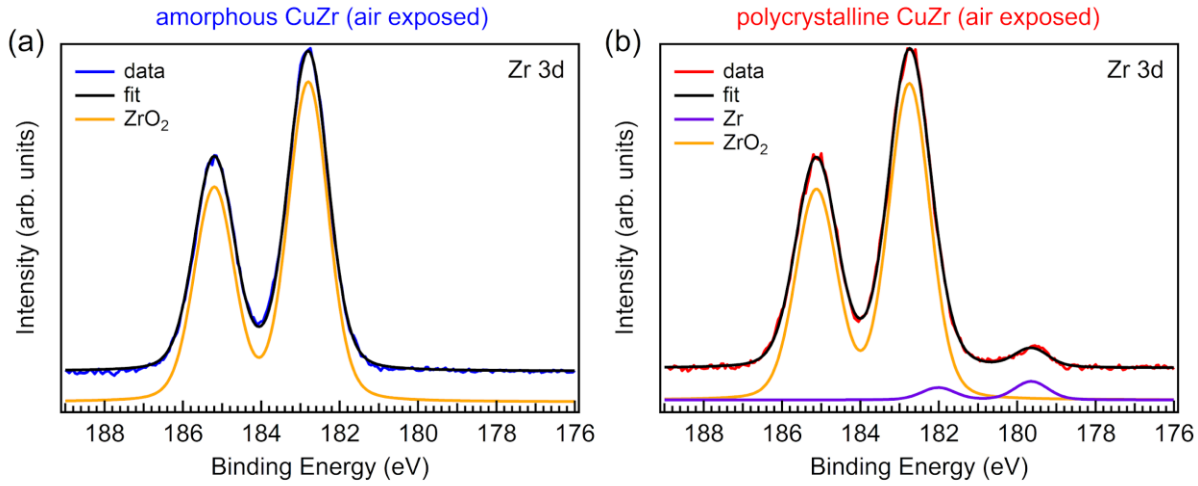

Figure S5: XPS measurements of the Zr 3d region for amorphous (a) and polycrystalline (b) CuZr thin films after air exposure. Both spectra display a main peak centred at E_B=182.8 eV ascribed to ZrO_2. The polycrystalline film shows the presence of an additional, low-intensity peak centred at E_B=179.5 eV and ascribed to metallic Zr.

Optical measurement of the band gap of amorphous CuZr

We determined the reflectivity of our thin films with Fourier transform infrared spectroscopy. Three experiments were performed that enabled us to determine the optical response of the polycrystalline and amorphous film. In the first experiment we determine the reflectivity of the bare, sapphire substrate, see Figure S6. Since the backside of the Al_2O_3(0001) substrate is unpolished, Fabry-Perot interference does not play a role in this experiment. We determine the reflectivity over

the energy range from 4 meV to 2.7 eV, using a combination of sources, beam-splitters and detectors described in [3]. We first determine the reflected intensity from the substrate and subsequently use evaporated gold (below 0.6 eV) or silver (above 0.6 eV) as reference to determine the absolute reflectivity. The excellent agreement between the reflectivity determined in different energy ranges and with different reference materials indicate an error on the reflectivity between 0.1% and 0.3%.

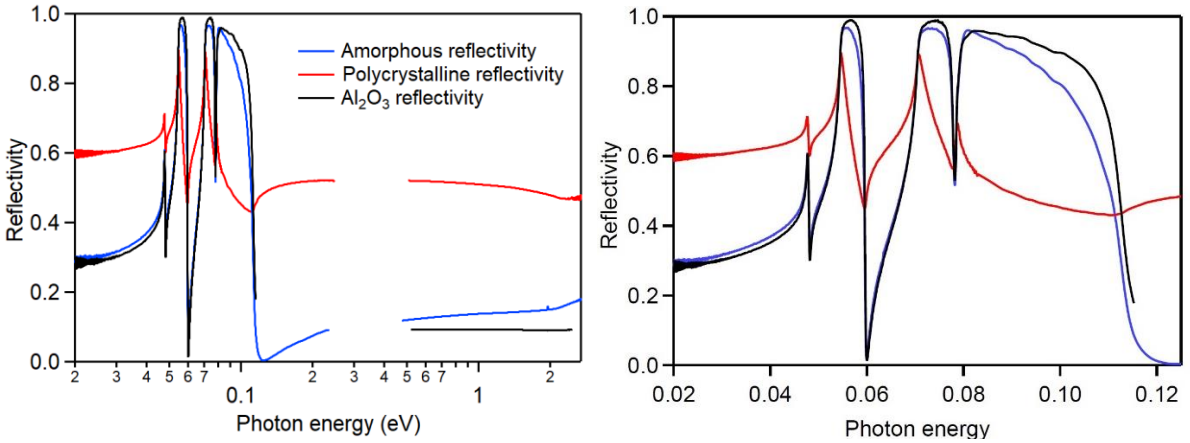

Figure S6: Full (left) and detailed (right) reflectivity data of amorphous (blue) and polycrystalline (red) layers of CuZr as well as an Al_2O_3(0001) reference sample (black) measured using FTIR.

The reflectivity of the substrate-film samples is determined in exactly the same way as the substrate. Comparing the three measurements in Figure S6, we see distinct difference between the bare substrate and the two substrate-film samples. Starting with the bare substrate, the reflectivity shows a series of infrared active phonon modes below 100 meV. The mode frequencies extracted from a Drude Lorentz model (see below) agree well with previously reported values [4]. Above 100 meV, the reflectivity is nearly frequency independent up to the limit of our energy range.

The reflectivity of the substrate with amorphous film is very similar to the bare substrate in the phonon energy range. The reflectivity in the NIR-VIS range of the spectrum is however significantly higher and acquires a frequency dependence. This points to an interband transition in this energy range. The reflectivity of the substrate with polycrystalline film is significantly different also in the far-infrared range. We still observe the same set of phonon modes, but they are significantly less pronounced. The NIR-VIS reflectivity is higher than both the amorphous film and substrate as could be expected from the distinctly different colour one can observe with the naked eye.

To extract the optical conductivity, we model the reflectivity date using RefFit[5]. In a first step we determine a Drude – Lorentz model that reproduces the reflectivity of the bare substrate. This is used as input in a model that solves the Fresnel equations for the combined substrate plus film data. In this model, the measured reflectivity is reproduced with the previously determined substrate model and a second model for the dielectric function of the film. From this analysis we can estimate the DC conductivities for both films. We find $\sigma_{DC} \approx 5.8\ m\Omega^{-1}cm^{-1}$ for the polycrystalline film and $\sigma_{DC} \approx 1.5 \times 10^{-1}\ m\Omega^{-1}cm^{-1}$ for the amorphous film.

Reproducing the measured reflectivity data for the amorphous film requires a single Lorentzian-like oscillator at high energy. This allows us to make an estimate of the bandgap of the amorphous film at approximately 1±0.1 eV (see Table S1).

Table S1. Drude-Lorentz model mode frequencies in meV. In this table, ω_p is the plasma frequency, γ(D) indicates the line broadening, ω_0 is the central frequency of the Lorentz oscillator or phonon mode and f_p is the corresponding oscillator strength. The phonon modes of the Al_2O_3 substrate correspond well with previously reported literature. The final row of the table indicates the estimated ε_∞, which is a measure of high-energy interband transitions above our energy range.

Sample		Al_2O_3	PC	Amorphous
Drude	ω_p	-	4849	-
	γ_D	-	511.4	-
Lorentz 1	ω_0	84.1	1463	806.4
	f_p	30.2	12072	2857
	γ	32.2	4252	3567
Phonon 1	ω_0	47.8	-	-
	f_p	23.7	-	-
	γ	0.1	-	-
Phonon 2	ω_0	54.5	-	-
	f_p	95.0	-	-
	γ	0.2	-	-
Phonon 3	ω_0	70.6	-	-
	f_p	127.6	-	-
	γ	0.3	-	-
Phonon 4	ω_0	78.6	-	-
	f_p	35.1	-	-
	γ	0.9	-	-
ε_∞		3.44	19.3	6.24

References

[1] I. Bespalov, M. Datler, S. Buhr, W. Drachsel, G. Rupprechter, and Y. Suchorski, *Initial Stages of Oxide Formation on the Zr Surface at Low Oxygen Pressure: An in Situ FIM and XPS Study*, Ultramicroscopy **159**, 147 (2015).

[2] M. C. Biesinger, *Advanced Analysis of Copper X-Ray Photoelectron Spectra*, Surf. Interface Anal. **49**, 1325 (2017).

[3] A. Tytarenko. Exploring instabilities of bad metals with optical spectroscopy. (2017)

[4] Y. Liu, B. Cheng, K. Wang, G. Ling, J. Cai, C. Song, G. Han. *Study of Raman spectra for γ-Al_2O_3 models by using first-principles method.* Solid State Communications **178**, 16 (2014)

[5] A.B. Kuzmenko*, Kramers–Kronig constrained variational analysis of optical spectra*. Rev. Sci. Instrum. **76**, 083108 (2005)